

# Optical Sensor Using Space-Domain Active Fiber Cavity Ringdown Technique

**Wenjia Chen**

Hubei University of Technology

**Yiwen Ou** (✉ [ouyiwen@hbut.edu.cn](mailto:ouyiwen@hbut.edu.cn))

Hubei University of Technology

**Chunfu Cheng**

Hubei University of Technology

**Yuanchang Zhu**

Hubei University of Technology

**Wen Xiao**

Hubei University of Technology

**Hui Lv**

Hubei University of Technology

---

## Research Article

**Keywords:** Optical sensor, space-domain, fiber cavity, ringdown technique, signal, magnetic field sensitivity

**Posted Date:** December 3rd, 2021

**DOI:** <https://doi.org/10.21203/rs.3.rs-1129426/v1>

**License:**  This work is licensed under a Creative Commons Attribution 4.0 International License.

[Read Full License](#)

---

# Optical sensor using space-domain active fiber cavity ringdown technique

Wenjia Chen,<sup>1,2</sup> Yiwen Ou,<sup>1,2\*</sup> Chunfu Cheng,<sup>1,2</sup> Yuanchang Zhu,<sup>1,2</sup>  
Wen Xiao,<sup>1,2</sup> Hui Lv<sup>1,2</sup>

<sup>1</sup>Hubei Engineering technology Research Center of Energy Photoelectric Device and System,  
Hubei University of Technology, Wuhan 430068, China;

<sup>2</sup>School of Science, Hubei University of Technology, Wuhan 430068, China

\*ouyiwen@hbut.edu.cn

**Abstract:** A novel active fiber cavity ringdown (FCRD) technique using frequency-shifted interferometry (FSI) is proposed for the first time. Using this scheme, external parameters can be monitored in the space domain by measuring the ringdown distance instead of ringdown time. A bidirectional erbium-doped fiber amplifier (Bi-EDFA) is employed to compensate the inherent cavity loss for achieving higher sensitivity. And two band-pass filters are used to reduce the amplified spontaneous emission (ASE) noise of the Bi-EDFA. Compared with the well-known time-domain active FCRD scheme, our proposed method enables us to avoid using pulsed laser needed in time-domain active FCRD, it uses continuous-wave laser to inject into the fiber cavity and stabilize the optical power in the fiber cavity, which can suppress gain fluctuations of the EDFA and thus improve the detecting precision. Moreover, this novel method enables us to use differential detection method for further reducing the ASE noise, and thus eliminating the baseline drift of ringdown signal. A magnetic field sensor was developed as a proof-of-concept demonstration. The experimental results demonstrate that the proposed sensor with a sensitivity of 0.01537 (1/km·Gs) was achieved. This is the highest magnetic field sensitivity compared to the time-domain active FLRD method. Due to the reduced ASE noise, the stability of the proposed sensing system was also greatly improved.

## Introduction

Fiber cavity ringdown (FCRD) sensing technique is a highly sensitive method for measuring optical losses [1]. Similar to conventional CRD scheme, the cavity loss can be determined from the decay rate usually called ringdown time of the pulsed laser. But unlike conventional CRD method, in which the light bounces back and forth between two mirrors, FCRD usually uses a pair of fiber directional couplers with high splitting ratio to form the fiber cavity for achieving the multi-pass approach. Compared to mirror-based cavity, a fiber cavity has the advantages of being alignment-free, robustness, low cost and suitable for large-scale, multi-function sensor network, which has made FCRD becoming a popular

choice for many applications such as gas [2], liquid [3], pressure [4], strain [5], temperature [6], magnetic field sensing [7] and so on. However, fiber cavity has its shortcoming of the large inherent cavity loss due to the large insertion loss of fiber couplers and sensor heads, which leads to a poor sensitivity.

In order to improve the sensitivity, one simple way to achieve this goal is to reduce the insertion losses of the sensor heads, but the improvement is still limited. Another approach is to compensate the inherent cavity loss by introducing an erbium-doped fiber amplifier (EDFA) to the fiber cavity. As the EDFA is served as the gain source, this new FCRD is usually named as time-domain active FCRD or amplified FCRD [8-18]. In 2001, the active FCRD technique was firstly proposed by George Stewart and the sensitivity was improved because the inherent cavity loss can be sufficiently compensated by the EDFA [8]. However, the active FCRD sensing method also brings two new problems. One is the gain fluctuation of the EDFA, which results in the nonexponential decay of the ringdown signal and thus degrades the measurement precision and long-term stability [17,18]. Another is the amplified spontaneous emission (ASE) noise produced by EDFA, which causes the baseline drift of ring-down signal and reduces the stability of the sensing system [9, 10, 14]. To minimize the impact of gain fluctuation, a gain clamped EDFA was used in the fiber cavity to reduce the gain fluctuation effect [11, 12], but the gain fluctuation still exists because the pulsed laser was used in time-domain active FCRD to excite the fiber cavity and thus it cannot provide the power stabilization in the fiber cavity, so the stability was usually only about 10% which was not suitable for the practical application [15]. Fortunately, a chaotic laser was proposed to stabilize the laser power in the fiber cavity and the gain fluctuation was effectively suppressed, therefore, a good stability of 2.84% was achieved recently [16]. In order to improve the stability, an adaptive filter was suggested to suppress the ASE noise [9, 10], however, it is impossible to completely eliminate it and thus the stability was still not sufficient.

Conventional FCRD method belongs to time-domain sensing technique because it usually uses pulsed laser to excite the fiber cavity and measures its decay rate (ringdown time) in the time domain. As this scheme is based on using an expensive pulsed laser, a fast detector and a fast data acquisition card (DAQ), it incurs high instrument costs and limits its applications. To solve the above issues raised by conventional FCRD scheme, a space-domain passive FCRD technique was proposed based on frequency-shifted interferometry (FSI), which usually called as FSI-FCRD [19-21]. This novel scheme does not rely on any time-domain

measurement of a decaying pulsed laser. Instead, it is able to deduce the cavity loss information by measuring the ringdown distance. Compared with the conventional FCRD method, this new scheme was more cost-effective because it utilizes a low-cost CW laser and slow detector without the need of expensive pulsed laser and fast electronics. Due to its excellent characteristics, such as low cost and high stability, the space-domain passive FCRD technique has attracted more and more interests and been widely used for many sensing applications, such as gas detection [22], pressure [23], magnetic field sensing [24] and so on. However, it has the same problem of large inherent cavity loss as the time-domain passive FCRD sensing method, which limits the sensitivity of the sensing system. To meet the requirements of many practical applications for high sensitivity, a space-domain active FCRD is urgently required to develop. However, to the best of our knowledge, it has not yet been reported.

In this paper, we proposed the space-domain active FCRD technique for the first time and successfully carried out proof-of-concept experiments to measure magnetic field. The experimental results show that this novel scheme can not only significantly increase the sensitivity, but it is able to improve the stability of sensing system due to the reduced gain fluctuation by using a CW source to stabilize the laser power in the fiber cavity. It is fundamentally different from the time-domain active FCRD technique since the latter requires pulsed laser to inject the fiber cavity and thus a large gain fluctuation is generated. This paper is organized as below. In section 2, we introduce the principle of the space-domain active FCRD. In section 3 and 4 we respectively show the experimental setup and experimental results of the space-domain active FCRD magnetic field sensing system. The last section is a short summary.

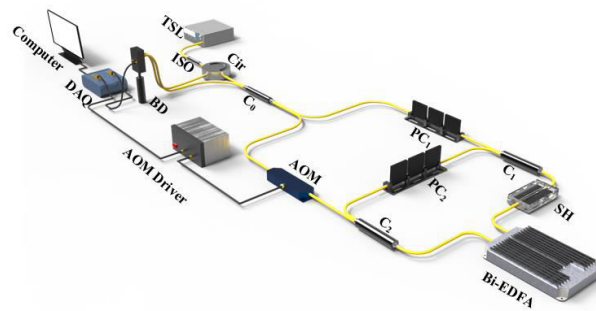


**Figure 1.** Schematic diagram of the space-domain active FCRD sensing system. TSL: tunable semiconductor laser; ISO: isolator; Cir: circulator;  $C_0$ : 3 dB fiber coupler;  $C_1$  and  $C_2$ : high splitting-ratio fiber couplers;  $PC_1$  and  $PC_2$ : polarization controllers; SH: sensor head; Bi-EDFA: bidirectional erbium doped.

## Principle

The schematic diagram of the space-domain active FCRD sensing system is depicted in Figure1. From Figure1 we can see that a Sagnac interference loop, with an asymmetrically-embedded frequency shifter, constitutes a frequency-shifted interferometer [25]. An active fiber cavity is composed by two fiber couplers ( $C_1$  and  $C_2$ ) with high splitting ratios, a sensor head (SH), a bidirectional erbium-doped fiber amplifier (Bi-EDFA), which is inserted into the frequency-shifted interferometer to form the space-domain active FCRD sensing system. The working principle of space-domain active FCRD sensing system can be described as follows. The CW light generated from the optical source (OS) is coupled into the frequency-shifted interferometer through the circulator (Cir) and the fiber coupler  $C_0$ . It produces two light beams circulating the fiber cavity in counter-propagating directions. A Bi-EDFA as shown in Figure 1 is incorporated into the fiber cavity to amplify the intensity of the two light beams in the cavity. Consequently, it compensates the inherent cavity loss, the light-sample interaction time is prolonged, and the two light beams attenuate more slowly. Small amounts of the light beams leak out from the fiber cavity and encounter in the coupler  $C_0$ , after completing each roundtrip in the cavity. As the length of the fiber cavity is set to be far larger than the source's coherence length, the interference occurs between the two light beams exiting from the fiber cavity after going through the same number of roundtrips. The differential interference signal at the BD can be described as [19, 20]

$$\Delta I \propto \sum_{m=0}^{\infty} I_m \cos \left[ 2\pi \frac{n(mL+L_0)}{c} f \right] = \sum_{m=0}^{\infty} I_m \cos(2\pi F_m f) \quad (1)$$

where  $n$  is the refractive index of the single-mode fiber,  $L$  is the length of the fiber cavity,  $L_0$  is a constant,  $f$  is the frequency shift generated by the frequency shifter,  $c$  is the propagation speed of the light in vacuum.  $F_m = n(mL+L_0)/c$  is the oscillation frequency that has a linear relationship with the roundtrip number  $m$ . As  $c$  is very large, the sensing system can work under the low oscillation frequency  $F_m$ , that is to say, slow detection is achieved using FSI and thus the cost is reduced.  $I_m$  is the intensity of the interference light after  $m$  roundtrips:

$$I_m = I_0 \cdot \exp(-m\alpha_0) = I_0 \cdot \exp\left(-\frac{l}{L}\alpha_0\right) \quad (2)$$

where  $I_0$  is the initial intensity,  $l = mL$  is the distance traveled by the light in the fiber cavity, and  $\alpha_0$  is the cavity loss, which contains the total fiber transmission loss  $\alpha_c$  and the gain  $G$  of the Bi-EDFA in the fiber cavity, and can be given by

$$\alpha_0 = \alpha_c - G = \alpha_{AR} + \alpha_{ST} + \alpha_{FS} + \alpha_{IR} - G \quad (3)$$

where  $\alpha_{AR}$  represents the fiber absorption loss,  $\alpha_{ST}$  is the fiber scattering loss,  $\alpha_{FS}$  is the fiber fusion loss, and  $\alpha_{IR}$  is the insertion loss of the components including the two fiber couplers, the polarization controller and the sensor head (SH).  $\alpha_c = \alpha_{AR} + \alpha_{IR} + \alpha_{ST} + \alpha_{FS}$  represents the inherent cavity loss, which is larger than the cavity loss  $\alpha_0$ .

As it can be seen from Eq.s (1)-(3),  $Im$  is an exponentially decay function of the propagation distance  $l$ , while  $Fm$  is a linear function of  $l$  according to the relation  $l = mL$ . Therefore, by linearly sweeping the frequency shift  $f$  and applying fast Fourier transform (FFT) to  $\Delta I$ , one can obtain the Fourier spectrum of  $\Delta I$  which display a series of exponentially decaying peaks located at  $F_m$ . After converting the frequency  $F_m$  to the propagation distance  $l'$  using the formula  $l' = l + L_0 = cF_m/n$ , the Fourier spectrum of  $\Delta I$  will become a ringdown transient as the propagation distance [19, 20], which indicates our proposed method belongs to a space-domain FCRD technique realized by using FSI scheme. The distance required for the light intensity to decrease to 1/e of the initial light intensity can be defined as the ringdown distance, which is analogous to the ringdown time [1]. When no external action applied on the SH, the ringdown distance  $\Lambda_0$  can be written as

$$\Lambda_0 = \frac{L}{\alpha_0} \quad (4)$$

When an external action  $P$  (magnetic field, pressure, strain, etc.) is applied on the SH, an additional loss  $\alpha_s$  occurs, which results in a change in the ringdown distance. In this case, the ringdown distance  $\Lambda$  can be rewritten as

$$\Lambda = \frac{L}{\alpha_c + \alpha_s - G} = \frac{L}{\alpha_c + \xi l_s P - G} \quad (5)$$

where  $\alpha_s = \xi l_s P$ ,  $\xi$  is the external-action-induced absorption coefficient [26], and  $l_s$  is the length of the SH. Combining Eq. (4) with Eq. (5), we have

$$\left(\frac{1}{\Lambda} - \frac{1}{\Lambda_0}\right) = \frac{\alpha_s}{L} = \frac{\xi l_s}{L} P = kP \quad (6)$$

Obviously, the external parameter is determined by measurement of ringdown distances  $\Lambda$  (with the external action applied) and  $\Lambda_0$  (without the external action applied), and the reciprocal difference  $(1/\Lambda - 1/\Lambda_0)$  of ringdown distance changes linearly with the change of the external action, for a given space-domain active FCRD sensor. The slope  $k = \xi l_s / L$  represents the sensor's sensitivity to the sensing activity, which can be tailored by adjusting the length of SH and the cavity length. Additionally, the detection limit is also an important indicator of system performance as well, which is defined as the minimum detectable external parameter  $P_{min}$ . It can be obtained by taking the derivation of both sides of Eq. (6)

$$P_{\min} = \frac{1}{kN_e L} \cdot \frac{\delta\lambda}{\bar{\lambda}} = \frac{S}{kN_e L} \quad (7)$$

where  $N_e = \Lambda_0 / L$  is the effective number of roundtrips traveled by the light within the ringdown distance  $\Lambda_0$ , which essentially represents the multiple rounds of interaction in the SH. Therefore, compared with the detection limit of an intensity-based fiber optic sensor, our proposed sensor will improve the detection limit by a factor of  $N_e$ .  $\delta\lambda$  and  $\bar{\lambda}$  denote the standard deviation and the averaged value of the ringdown distance under the condition of no external action applied on the SH, respectively. The ratio  $\delta\lambda / \bar{\lambda}$  can be defined as the stability  $S$  of the proposed sensing system. Equation (8) indicates that the high detection limit can be expected under the good stability, which is very important to the practical application. As the gain of Bi-EDFA can decrease the cavity loss and prolong the ringdown distance, the space-domain active FCRD technique will have larger effective circulating number and thus results in a higher sensitivity and detection limit. However, a higher sensitivity usually results in a smaller dynamic range, and vice versa [27]. That is to say, they should be compromised according to the requirements of the practical applications.

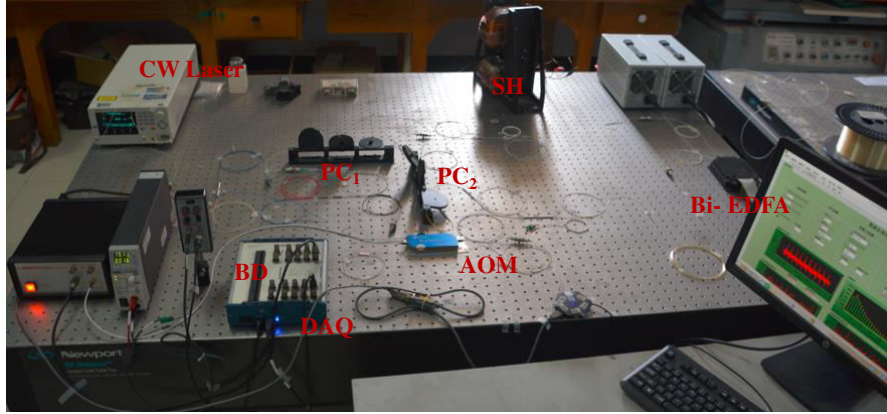


**Figure 2.** The experimental setup of the space-domain active FCRD magnetic field sensing system.

## Experimental setup

In order to verify the feasibility of our proposed concept, a space-domain active FCRD sensing system was constructed for magnetic field measurement as shown in Figure 2. A tunable semiconductor laser (TSL, Santec TSL-550) was employed to generate CW light. During the magnetic field sensing experiments, the output power of TSL was set to 9 mW at 1530.37 nm. An acousto-optic modulator (AOM, Brimrose, AMM-100-20-25-1550-2FP) served as the frequency shifter, and its sweeping frequency was set to rise from 90 to 110 MHz with a 0.02 MHz increment each time. Two fiber couplers with a splitting ratio of

99.5:0.5 constituted the fiber cavity with a length of ~ 130 m. Two polarization controllers ( $PC_1$  and  $PC_2$ ) were used to optimize the polarization state of the CW light for obtaining the visible interference fringe. The differential interference signal was detected by the balanced detector (BD, New Focus Model 2117), and then recorded by a data acquisition card (DAQ, NI USB-6361) at a sampling rate of 100 kS/s. Note that this detection speed is much slower than that of conventional time-domain FCRD sensing system [1,13]. The collected signal was then transmitted to the desktop computer and processed by a Labview program in real time.

As a proof-of-principle demonstration, we introduced the cavity loss induced by magnetic field, and a side-polished fiber (SPF) coated with magnetic fluid (MF) was utilized as the SH (see Figure 3(b)) for magnetic field sensing. The SPF (Micro photons Technology Co., NIR-SPF-W1550-2) was fabricated by side polishing the cladding of a single-mode fiber to 5-6  $\mu\text{m}$  from the core as illustrated in Figure 3(a), which significantly enhanced the evanescent field effect in the polished area with a length of 17 mm. Compared with the tapered fibers, the SPF has stronger mechanical strength because the other side of the fiber is intact. Moreover, the fabrication method requires no pigtailling and no intrusion into the core of the fiber, which produces a robust structure. Then the SPF was encapsulated in a plexiglass box filled with the MF (Water-based Ferrofluid, EMG-603P, Ferrotec (USA) Corp.). The MF was a stable water-based ferrofluid with  $\text{Fe}_3\text{O}_4$  as the magnetic nanoparticles. Due to the agglomeration of  $\text{Fe}_3\text{O}_4$  particles and formation of a long-chain structure that is parallel to the magnetic field direction [28], the refractive index and absorption coefficient of MF will change with the change of the ambient magnetic field strength. When the magnetic field was applied on the proposed SH, a magnetic-field-induced cavity loss will emerge, which results in the change of the ringdown distance. Consequently, the applied magnetic field can be measured by monitoring the change in ringdown distance. The two small holes on the top of the plexiglass box was packed with paraffin to prevent the MF from overrunning the box. A self-made magnetic field generating device created the magnetic field in the experiments, which was composed by two square iron cores wound tightly with copper wire and fed by a digital regulated DC power supply. The direction of the magnetic field was perpendicular to the propagation direction of the CW light in the fiber cavity. A gaussmeter (Pafei Hangzhou, BST-801) was employed to measure the magnetic field as a benchmark.

It is worth noting that the EMG-603P MF used here wasn't diluted using distilled water as in our recent work [29]. The space-domain ringdown event couldn't be observed anyway before connecting the Bi-EDFA inside the fiber cavity, which indicates that high concentration of MF causes a large cavity loss. However, after a customized Bi-EDFA (Tianjin Junfeng Technology Co., EDFA-WDM-C-MB) was utilized to realize the bi-directional amplification of the CW light intensity, the space-domain ringdown transient could be observed immediately. It experimentally reveals that the Bi-EDFA can compensate the cavity loss and prolong the ringdown distance. Two band pass filters were encapsulated in the Bi-EDFA to filter out the ASE noise, each with a central operating wavelength of 1,530.33 nm and a 3 dB bandwidth of 0.8 nm. The pump current of the Bi-EDFA were set to 135 mA during the experiments.

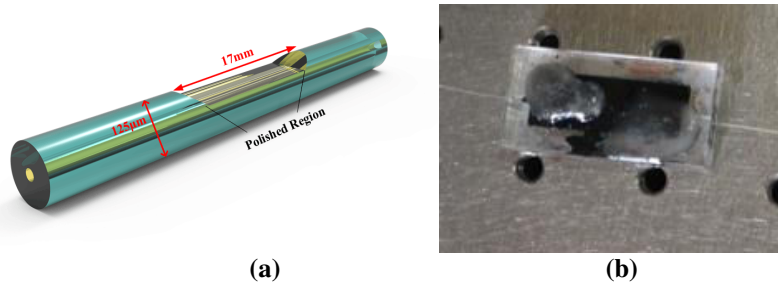


**Figure 3.** (a) Schematic diagram of the side-polished fiber; (b) Physical view of the magnetic field sensor head.

## Results and discussion

A typical differential interference signal is shown in Figure 4(a) when there was no external magnetic field was applied on the SH, and the corresponding ringdown waveform in the space domain (see Figure 4(b)) was obtained after taking FFT of the differential interference signal. The peaks on the ringdown signal can be extracted by applying a peak extraction algorithm. By fitting these peaks with an exponential (EXP) function, an exponential decay curve was obtained. Then the ringdown distance was calculated out to be 1,027.92 m according to its definition, and cavity length was  $\sim 128.78$  m by calculating the average space interval between two adjacent peaks. According to Eq. (4) the cavity loss can be deduced to be 0.548 dB in the absence of an external magnetic field.

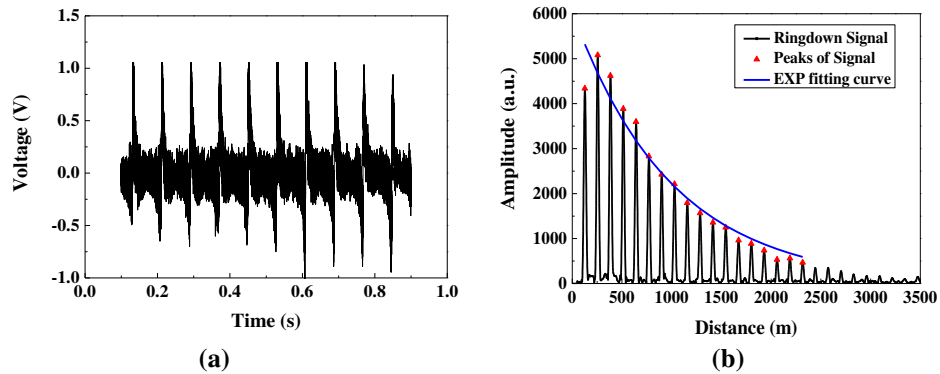


**Figure 4.** The typical signals measured by the space-domain active FCRD technique. (a) the time-domain differential interference signal; (b) the corresponding ringdown transient in the space domain.

To characterize the response of the proposed sensing system to magnetic field and evaluate its sensitivity, the magnetic fields ranged from 0 to 170 Gs were applied on the SH, and the ringdown signals were measured. The obtained results are illustrated in Figure 5 (a). By using peak extraction algorithm and EXP fitting algorithm, the obtained exponential decay curves under different magnetic field strengths are depicted on Figure 5(b). As the magnetic field strength rises, the attenuation of the ringdown signal becomes faster, which shows the ringdown distance decreases with the increase of the magnetic field strength. This is because: when there is no magnetic field applied, the magnetic nanoparticles are uniformly distributed

in the carrier liquid; whereas when the magnetic field is applied, the magnetic nanoparticles gradually cluster along the direction of the magnetic field. As the intensity of the magnetic field increases, more and more magnetic nanoparticles are arranged into short-chain and long-chain structures, causing the increase in the refractive index of the MF [28]. As a result, more evanescent wave leaks out from the SPF, the cavity loss increases, and thus the ringdown distance decreases. This result can also be clearly observed in Figure 6, in which the measurement was repeated 30 times under each magnetic field strength to reduce the measurement errors. By calculation, the average ringdown distance measured by the sensing system reduced from 1,016.67 m to 313.42 m. To clearly demonstrate the response characteristics of our proposed sensing system, the relationship between the reciprocal

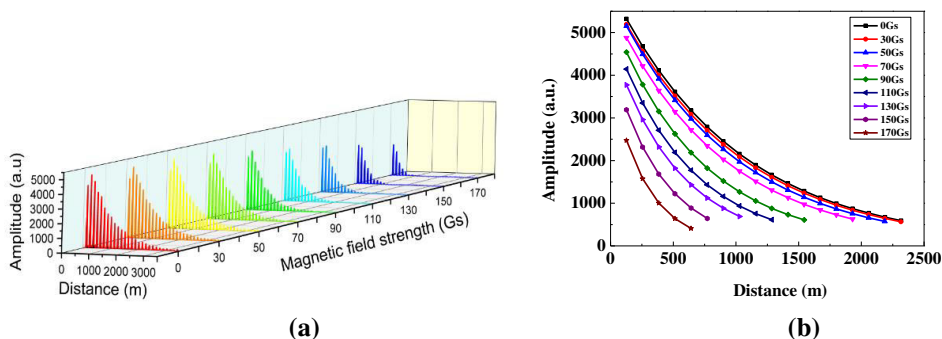


**Figure 5.** (a) the ringdown signals under the magnetic field strengths ranged from 0-170 Gs, (b) the corresponding exponential decay curves.

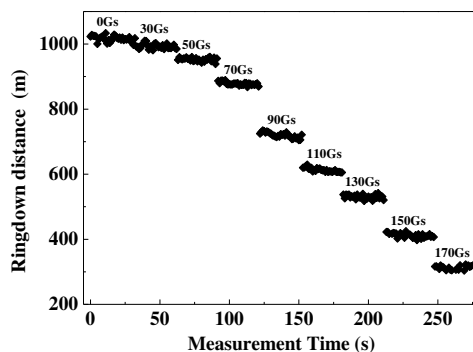


**Figure 6.** Ringdown distance versus magnetic field strength.

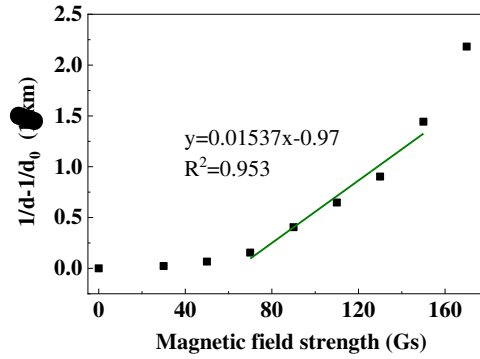


**Figure 7.** Reciprocal difference of ringdown distance as a function of magnetic field strength.

difference of ringdown distance ( $1/\Lambda-1/\Lambda_0$ ) and the magnetic field strength  $H$  was plotted as shown in Figure 7. As the magnetic field strength increases, the reciprocal difference of ringdown distance gradually increases. Through linear fitting, it can be found that, in the range of 70-150 Gs of magnetic field intensity, the linear fitting degree R-squared reaches 0.9530. It indicates that the sensing system has a good linear response, which also agrees well with the theoretic result described in Eq. (6). Other regions show a non-linear change trend, which mainly caused by the non-linear dependence of the MF's refractive index on the small magnetic field strength [7], and when the applied magnetic field strength exceeded 150 Gs, excessive cavity loss induced by magnetic field resulted in an unfaithful measurement and even the disappearance of the ringdown signal. Although the linear response range is limited, a highly sensitivity would be expected as a smaller measurement range usually results in a higher sensitivity. The fitted slope is 0.01537, which represents that the sensitivity of the sensing system is  $1.537 \times 10^{-2}$  (1/km·Gs). By converting ringdown time/distance change into cavity loss change for keeping units the same, it can be found that the sensitivities of the time-domain passive FCRD magnetic field sensors reported in [30], the time-domain active FCRD magnetic field sensing system [28], and the space-domain passive FCRD magnetic field sensing system [24] were all lower than the sensitivity of our proposed sensing system as shown in table 1. Obviously, the sensitivity of the space-domain active sensing system can be further enhanced by increasing the gain of Bi-EDFA, but large gain will bring a higher ASE noise, which will deteriorate the stability of the sensing system. In addition, according to the Eq. (6) the sensitivity also can be further improved by increasing the length of the SH, but the measurement range will be compromised. Therefore, the sensitivity and measurement range of the proposed sensing system should be tailored according to the specific performance requirements of the practical applications.

**Table 1 Comparison with conventional FCRD techniques.**

Ref.	Technique	Sensor head configuration	Sensitivity
[30]	Time-domain Passive FCRD	Fiber collimator lens and MF film	$1.94 \times 10^{-4}$ dB/ Gs
[28]	Time-domain Active FCRD	MF-coated U-bent SMF	$2.08 \times 10^{-3}$ dB/ Gs
[24]	Space-domain Passive FCRD	Etched fiber taper coated with MF	$1.05 \times 10^{-3}$ dB/ Gs
Our work	Space-domain Active FCRD	MF-coated side-polished fiber	$8.59 \times 10^{-3}$ dB/Gs

Finally, the stability of the sensing system was also tested. The ringdown distance was repeatedly measured one hundred times when no magnetic field was applied on the SH, and the results were demonstrated in Figure 8. The obtained mean ringdown distance was 1,019.27 m, and the standard deviation was 8.089 m. According to the definition of the stability in Section 2, the stability of 0.79% was obtained, which is much better than that of the time-domain active FCRD sensing system with stability around 10% [1, 10, 15] and also better than that of chaotic correlation FCRD sensing system with stability of 0.846% by using chaotic laser instead of pulsed laser to effectively suppress the gain fluctuations of EDFA [16]. The better stability of the proposed sensor system is attributed by the use of a CW light source to ensure the power stability in the fiber cavity for suppressing the gain fluctuations of the Bi-EDFA, the usage of differential detection to eliminate DC noise, and the essence of common-path interference to cancel common-mode noise. According to Eq. (7), the calculated detection limit of the proposed sensing system was 0.504 Gs, which is better than that of the FCRD-based magnetic field sensor reported in [29, 31]. In addition, the effective number of roundtrips  $N_e$  was calculated to be about 8, which means 8 rounds of interaction in the SH. In other words, the detection limit is about 8-fold enhancement than those of the conventional intensity-based sensors.

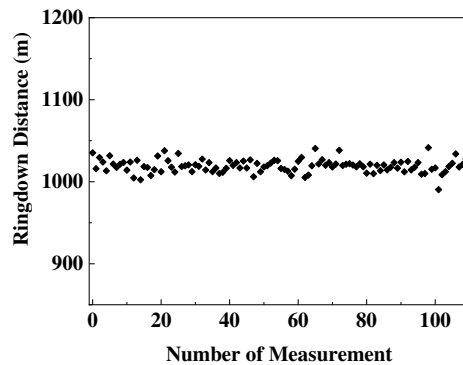


**Figure 8.** Stability measurement results of the proposed sensing system.

## Conclusions

In this paper, a space-domain active FCRD sensing technique by introducing the Bi-EDFA to compensate the inherent cavity loss was firstly proposed, and magnetic field sensing experiments were conducted to verify the concept. Compared to the conventional time-domain active FCRD scheme, this novel method does not need a pulsed laser and a fast detector, which reduces the system cost. It uses a CW laser to stabilize the laser power in the fiber cavity, and thus effectively suppress the gain fluctuations of the Bi-EDFA, offering a good stability for the sensing system. It also utilizes the different detection method to obtain high signal-to-noise ratio, and hence the stability of sensing system is further improved. In the magnetic field sensing experiments, we have achieved a highly sensitivity of  $1.537 \times 10^{-2}$  (1/km·Gs) and a good stability of 0.79%, both of which are better than those of time-domain active FCRD magnetic field sensing systems. The results show that the proposed method is cost-effective and suitable for many practical applications where high sensitivity and good stability are required.

## References

- 1 C. Wang, Fiber Loop Ringdown — a Time-Domain Sensing Technique for Multi-Function Fiber Optic Sensor Platforms: Current Status and Design Perspectives, *Sensors* **9**(10), 7595-7621 (2009).
- 2 X. Qian, Y. Zhao, Y.-n. Zhang, and Q. Wang, Theoretical research of gas sensing method based on photonic crystal cavity and fiber loop ring-down technique, *Sensors and Actuators B: Chemical*, **228**, 665-672 (2016).
- 3 Y. Jiang, et al, Precise measurement of liquid-level by fiber loop ring-down technique incorporating an etched fiber, *Opt. Commun.* **351**, 30-34 (2015).
- 4 C. Wang, S. T. Scherrer, Fiber ringdown pressure sensors, *Opt. lett.* **29**(4), 352-354 (2004).
- 5 P. B. Tarsa, D.M. Brzozowski, P. Rabinowitz and K. K. Lehmann, Cavity ringdown strain gauge, *Opt. lett.* **29**(12), 1339-1341 (2004).
- 6 C. Wang and A. Mbi, An alternative method to develop fibre grating temperature sensors using the fibre loop ringdown scheme, *Meas. Sci. Technol.* **17**, 1741-1751 (2006).
- 7 Q. Wang, et al, Magnetic field sensing based on fiber loop ring-down spectroscopy and etched fiber interacting with magnetic fluid, *Opt. Commun.* **356**, 628-633 (2015).
- 8 G. Stewart, K. Atherton, H. Yu, B. Culshaw, An investigation of an optical fibre amplifier loop for intra-cavity and ring-down cavity loss measurements, *Meas. Sci. Technol.* **12**(7), 843-849 (2001).
- 9 N. Ni, C. C. Chan, Improving the measurement accuracy of CRD fibre amplified loop gas sensing system by using a digital LMS adaptive filter, *Meas. Sci. Technol.* **17**(8), 2349-2354 (2006).
- 10 N. Ni, C. C. Chan, T. K. Chuah, L. Xia, P. Shum, Enhancing the measurement accuracy of a cavity-enhanced fiber chemical sensor by an adaptive filter, *Meas. Sci. Technol.* **19**(11), 115203 (2008).

- 11 H. Waechter, J. Litman, A. H. Cheung, J. A. Barnes, H. Loock, Chemical Sensing Using Fiber Cavity Ring-Down Spectroscopy, *Sensors*, **10**(3), 1716-1742 (2010).
- 12 N. L. Andrews, J. Litman, D. Stroh, J. A. Barnes, H. Loock, Near-infrared absorption detection in picolitre liquid volumes using amplified fibre loop ring-down detection, *Opt. Fiber Technol.* **19**(6), 822-827 (2013).
- 13 Y. Zhao, et al, Novel gas sensor combined active fiber loop ring-down and dual wavelengths differential absorption method, *Opt. Express*, **22**(9), 11244-11253 (2014).
- 14 C. Cheng, et al, Theoretical investigation on the effect of ASE noise for amplified fiber loop ring-down gas sensing, *Proceedings of the Spie* 101580 (2016).
- 15 K. Sharma, et al, Comparison of detection limit in fiber-based conventional, amplified, and gain-clamped cavity ring-down techniques, *Opt. Commun.* **407**, 186-192 (2018).
- 16 J. Yang, et al, The stability of chaotic correlation fiber loop ring down system with loss compensation, *IEEE Photon. Technol. Lett.*, **31**(6), 471-474 (2019).
- 17 T. Chu, P. Wang and C. Zhu, Modeling of active fiber loop ring-down spectroscopy considering gain saturation behavior of EDFA, *J. Lightwave Technol.* **38**(4), 966-973 (2020).
- 18 T. Chu, C. Zhu and P. Wang, Modeling of active fiber loop ring-down spectroscopy considering non-linear effects of EDFA gain, *IEEE Sensors J.* **21**(3) 3155-3162 (2021).
- 19 F. Ye, B. Qi, L. Qian, Continuous-wave fiber cavity ring-down measurements using frequency-shifted interferometry, *Opt. Lett.* **36**, 2080-2082 (2011).
- 20 F. Ye, C. Zhou, B. Qi, and L. Qian, Continuous-wave cavity ring-down evanescent-field sensing with a broadband source based on frequency-shifted interferometry, *Sensors and Actuators B: Chemical*, **184**, 150-155, 2013
- 21 W. Huang, et al, A Multichannel Spatial-Domain Fiber Cavity Ringdown Pressure Sensor, *IEEE Sensors Journal*, **20** (1), 441-447 (2020).
- 22 C. Cheng, et al, Simultaneous Measurement of Gas Composition and Concentration Combined Fiber Cavity Ringdown and Frequency-shifted Interferometry, *Opt. Fiber Technol.* **48**: 303-307 (2019).
- 23 Y. Ou, et al, Continuous-Wave Fiber Cavity Ringdown Pressure Sensing Based on Frequency-Shifted Interferometry, *Sensors*, **18**(4), 1207 (2018).
- 24 H Tian, C. Zhou, D Fan, Y Ou, and J. Yin, Continuous-wave fiber cavity ringdown magnetic field sensing method based on frequency-shifted interferometry, *Chin. Opt. Lett.* **12**, 120604 (2014).
- 25 F. Ye, Y. Zhang, B. Qi and L. Qian, Frequency-Shifted Interferometry — A Versatile Fiber-Optic Sensing Technique, *Sensors*, **14**, 10977-11000 (2014).
- 26 Q. Wang, et al, Magnetic field sensing based on fiber loop ring-down spectroscopy and etched fiber interacting with magnetic fluid, *Opt. Commun.* **356**, 628-633 (2015).
- 27 M. Ghimire, C. Wang, Highly sensitive fiber loop ringdown strain sensor with low temperature sensitivity, *Meas. Sci. Technol.* **28**, 105101 (2017).
- 28 Y. F. Chen, T. G. Liu, Q. Han, W. C. Yan, L. Yu, Fiber cavity ring-down cavity integrated U-bent single-mode-fiber for magnetic field sensing, *Photonics Res.* **4**(6), 322-326 (2016).
- 29 C. Cheng, et al, Fiber loop ring-down magnetic field sensor using frequency-shifted interferometry and D-shaped fiber coated with magnetic fluid, *IEEE Magnetics Letters*, **12**, 8100705 (2021).
- 30 Q. Wang, et al, A Novel Current Sensor Based on Magnetic Fluid and Fiber Loop Cavity Ringdown Technology, *IEEE Sensor Journal*, **15**(11), 6192-6198 (2015).
- 31 Y. Ou, et al, Multipoint magnetic field measurement based on magnetic fluid and FSI-FLRD, *IEEE Sensors Journal*, **21**(16), 18249-18255 (2021).

## Acknowledgement

National Natural Science Foundation of China (Grant Nos. 61805075, 61475044); Outstanding young and middle-aged science and technique innovation team of colleges and universities in Hubei province (No. T201907).

## Author contributions

W.Y.O., and F.C.C. supervised the work and conceived the aim of the research, J.W.C. conducted all experiments, C.Y.Z., and W.X. analyzed the results, W.Y.O., F.C.C and J.W.C. prepared a draft of the manuscript. All authors reviewed the manuscript.

## Competing interests

The authors declare no competing interests.